PILOT MODELLING FOR BOUNDARY HAZARD PERCEPTION AND REACTION STUDY

Linghai Lu[1] and Michael Jump[2]

[1]Senior Lecturer, Liverpool John Moores University, Liverpool, UK; Email: l.lu@ljmu.ac.uk
[2]Senior Lecturer, University of Liverpool, Liverpool, UK; Email: mjump1@liverpool.ac.uk

Abstract

Hazard perception is the recognition of conditions that may pose threats to the safety of flight. Recognizing hazards early is important since it gives you time to react or plan appropriate defensive action well before any actual danger materializes. This paper presents the development and subsequent analysis of a pilot model in order to understand, explain, and predict the pilot boundary-hazard perception and associated reactions. Hess's multi-loop pursuit pilot model has been used to develop the part of the pilot model that performs the primary tracking task. The influence of the hazard perception and its reaction on the primary task can be modelled as a positive-feedback lead-lag term with two dependent parameters – a lead visual equalization term and a control gain to characterize the severity of the hazard situation. The piloted-simulation results on the 3DOF Bo105 longitudinal model have a good agreement with those of theoretically predicated ones using the proposed pilot model in terms of the pilot cut-off frequency and the tracking performance. The research indicates that a certain high level of the hazard can increase the tracking performance if the pilot chooses appropriate visual-lead and control efforts. Moreover, the results also show that the similar tracking performance can be achieved subject to different levels of hazards at the cost of slightly increased control efforts.

Nomenclature

$E, \dot{E}$ = position and rate tracking error
f = task interference modelling factor between control axes
$G_{\delta\delta}$ = auto spectrum of a signal
$M, \dot{M}$ = position and rate outputs
n_w = white noise in visual cueing model
n = number of control channels
k_{agress} = pilot control activity aggression factor
K, K_m = boundary tracking feedback gain and its maximum value
K_p, K_r = pilot gains in the position and rate feedback loops respectively
q = pitch rate, rad/s
s = Laplace operator
t = time, s
u, w = velocities in the body x and z axis respectively, ft/s, ft/s
$x, \dot{x}$ = distance to and closure rate to a boundary, ft, ft/s
$\ddot{x}$ = acceleration in the Earth x axis, ft/s^2
X = Laplace transform of Δx
Γ = Laplace transform of $\Delta\tau$
δ_{lon} = longitudinal control input, in
ζ_{nm} = neuromuscular damping ratio
θ = pitch attitude, deg
θ_d = boundary size, deg
σ_{vis} = variance of white noise in visual cue model associated with visual cue quality
σ_{task} = variance of white noise in visual cue model associated with piloting task
τ = optical tau, the instantaneous time to contact boundary in the optical field, s
τ_{dp} = perception time delay, s
τ_{max} = time to boundary when the pilot applies maximum control input, s (Gray's model)
τ_{min} = time to boundary when the pilot first responds to the boundary with a control input, s (Gray's model)
ω_c, ω_{cut} = crossover frequency and pilot cut-off frequency, rad/s, rad/s
ψ_{tot} = total root-mean-square value of a signal
ω_d, ω_n = forced frequency and natural frequency, rad/s, rad/s
ω_{nm} = neuromuscular natural frequency, rad/s
ω_u = neutral stability frequency, rad/s

Subscripts

0 = initial values
b = boundary
i = iteration number

1. Introduction

Representative models of the human pilot are a key element for flying qualities, stability and control, aircraft-pilot coupling, and simulation fidelity analyses. As such, they can help to improve flight safety [1-3]. The authors, in Ref. [4], have implemented pilot modelling techniques to study adverse aircraft-pilot coupling phenomena. The coupled aircraft-pilot-control system showed stability characteristics such that strong control of one part of the system may drive another part unstable [5;6]. It is well known, for example, that Pilot Induced Oscillations (PIOs) can result from the pilot increasing his/her control gain during a point tracking

(PT) task [4]. As modern aircraft become more sophisticated and need to operate over a wider range of mission tasks, the level of interaction between the flight control system and the pilot is likely to increase. Further development of pilot modelling techniques are therefore required to gain a better understanding of this interaction and how it might affect the vehicle's handling qualities [7].

The traditional view of how pilots perform a wide range of flying tasks involves an initial acquisition and then point tracking (PT) of the aircraft's flight path or attitude [2;4], such as when air-to-air refuelling, target tracking, formation flying, or in the presence of disturbed atmospheric conditions. However, there are times when a pilot controls the aircraft to avoid a hazard rather than hold a particular flight condition. This kind of hazard can be any constraint or boundary that requires the pilot to change the aircraft's flying state (e.g., altitude, airspeed, heading, route of flight, or configuration) to maintain the safety of the vehicle. By deviating from the PT task, pilots have been posited to adopt a strategy that focuses upon the monitoring and avoidance of one or more of these boundaries. Gray first described this phenomenon as a Boundary Tracking (BT) strategy [8]. For example, a pilot may encounter a situation whereby s/he is simultaneously trying to avoid a ground impact whilst, at the same time, preventing a low-altitude departure from controlled flight at an angle-of-attack limit. Boundary Tracking was further classified into Boundary Avoidance Tracking (BAT) and Boundary Escape Tracking (BET) depending upon whether or not the boundary in question represented a survival threat to the pilot (BAT: no; BET: yes). If a PIO were to arise from these situations, then these were proposed as 'Boundary-driven' PIOs and denoted BAT PIO or BET PIO as appropriate. BAT and BET PIOs have been observed to occur and are distinct from classical PT PIOs [8].

The authors' previous research in Ref. [9] has extended Gray's concept to cover PT-dominant situations, subject to a BA influence as a secondary, managerial task [10;11]. For example, ADS-33E Mission Task Elements [12], by having boundaries associated with desired and adequate handling qualities performance criteria (which may not be associated with a dangerous boundary), are examples of potential PT-dominant tracking tasks with a BA element. A skilled and experienced pilot has normally been well trained to deal with situations involving simultaneous primary PT control and secondary managerial tasks. The pilot is able to allocate attention to multiple tasks in which information is simultaneously gathered from a number of perceptual fields. Therefore, as far as the active BT pilot control processes are concerned, the PT (primary task) and BA (secondary task) may run concurrently, at least for a certain period after the initiation of the BA task i.e. the PT and BA perceptual inputs impinge and are acted upon by the pilot at the same time.

Poor pilot perception of and subsequent reaction to hazards are identified as an important factor in a large percentage of fatal aviation accidents, especially in general aviation (GA) [13]. This can be a particular problem in rotorcraft because their flying operations often take place at low altitude and in spatially confined areas (e.g. ship landing) or in poor visibility [14]. As a consequence, rotorcraft pilots are more susceptible to potential boundary hazards (e.g., during Nap-of-the-Earth flight). The authors' previous research in Ref. [9] has indicated that the closed-loop stability of the pilot-vehicle system can deteriorate when the pilot reacts to the impending boundary. It is therefore considered to be important to study and understand the pilot's control behaviour associated with the awareness of and consequent response to this kind of hazard detection and avoidance scenario. This will be the focus of the paper. First, the PT pilot model will be validated using real piloted-simulation data. Second, the research presented will extend the special boundary limits assumed in the previous work to a more generic hazard situation. Third, the control information used when the pilot-vehicle system is moving toward a hazard will be studied. Finally, the pilot reaction mechanism to a hazard will be investigated in a systematic way.

The paper proceeds as follows. The Hess multi-loop pursuit pilot model is reviewed in Section 2. The detailed experiment setup is presented in Section 3. In Section 4, results from a piloted pitch-tracking task, conducted in a flight simulation facility are investigated and discussed. Finally, the paper ends with the conclusions drawn from the work.

2. Pilot Modelling for Boundary Hazard Perception

The research reported here extends the authors' previous research [9] by proposing a multi-loop pilot model with a hazard-avoidance (HA) feedback loop as illustrated in Figure 1.

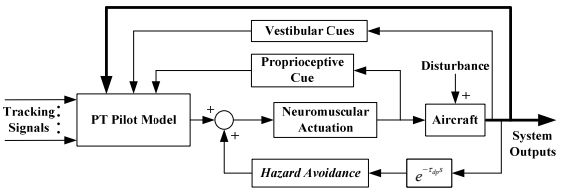

Figure 1 Closed-loop pilot model with the hazard avoidance feedback

The proposed pilot model of Figure 1 consists of two functions: the PT part, which models the pilot behaviour when performing classical, closed-loop tracking tasks, and the HA part, which models the pilot control activity/effort after recognition of potential hazards. A perception time delay τ_{dp} has been introduced in the HA loop to account for the delays associated with the pilot's inherent-delay response and with the visual perception

process. These two functions, as well as those additional blocks in Figure 1, will be elaborated upon in this section.

2.1 Modelling of Performing Tracking Tasks

Hess's multi-loop pursuit pilot model has been shown to be "representative" of a real pilot for use in simulations of realistic flight tasks. It takes account of a number of practical factors such as the effects of task interference between the different control axes, motion and visual cues, and the level of pilot control aggressiveness and skill [3;15-17]. The procedure proposed by Hess for modelling pilot pursuit control behaviour has shown significant value for research. The pilot model created is not only able to describe pilot pursuit behaviour, but can also account for visual, proprioceptive, and vestibular cues in an approximate fashion [15;16;18;19]. Therefore, this pilot model is extended in the current work to design a PT pilot model that performs the tracking task.

As a starting point, the structure of the multi-loop pilot model is illustrated in Figure 2

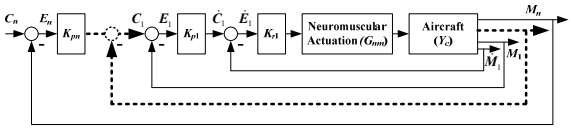

Figure 2 Hess' loop-by-loop pursuit pilot model [15]

Figure 2 describes a pilot model consisting of *n*-pair inner (output rate feedback, $\dot{M}_i$) and outer (output position feedback, M_i) loops. These position-based loops (C_i and M_i) and their first-order derivatives ($\dot{C}_i$ and $\dot{M}_i$) are closed because they are usually available to the pilot during a manoeuvring task. The outer loop of each pair (C_i and $\dot{C}_i$) deals with the feedback position error (E_i) between a given tracking signal (C_i) and feedback position (M_i). For example, the first inner-most loop deals with the tracking position error (E_1), through the gain variable K_{p1}, between the first output position feedback (M_1) and the reference signal (C_1), generated from the next-outer loop. Similarly, the inner loop of each pair addresses the rate feedback information. The inner loop represents the extra control effort that the pilot may apply due to possible additional cognitive information [5]. Besides these loops, the neuromuscular system (G_{nm}) of the pilot is modelled as a second-order transfer function by neglecting very-high frequency input information [15;16]:

$$G_{nm} = \frac{\omega_{nm}^2}{s^2 + 2\zeta_{nm}\omega_{nm}s + \omega_{nm}^2} \quad (1)$$

in which ζ_{nm} is the neuromuscular damping ratio and ω_{nm} its natural frequency. Moreover, the rate and position information mentioned above is described in a relative manner. They can refer to various sources that a pilot is able to sense. For example, the rate feedback may be based upon proprioceptive and vestibular cues. When these cues are required for the pilot model, ad-hoc techniques are used to model the sensory systems. The details relating to the work reported in this paper will be provided as required hereafter. When visual cues are being used, the following visual model [19] is adopted on each visual channel to reflect the quality of visual information sensed by the pilot:

$$E_i' = E_i(1+n_w)\frac{1}{0.5s+1} \quad (2)$$

in which n_w is a zero-mean, normally distributed random variable with variance σ_{vis}. E_i is the position tracking error of the i^{th}-pair feedback loop. This equation also applies to the rate tracking error ($\dot{E}_i$), if sensed by the pilot. This signal is saturated with limits $2\sigma_{\text{vis}}$. The better the useable cue environment, the lower is the value of σ_{vis}.

The successful implementation of the multi-loop pilot model depends upon a sensible selection of the pilot gains in Figure 2. It needs to satisfy at least 2 requirements. First, the final pilot model should be able to perform the required tracking task. Second, the pilot model should match the real behaviour of a pilot as closely as possible. This is unlike the approach of simply using PID controllers, where the aim is to achieve the tracking performance as accurately as possible. To meet these requirements, the following rules are used to select pilot gains (starting from the inner-most loop). The gain K_{r1} is chosen such that all of the damping ratios of the transfer function $\dot{M}_1/\dot{C}_1$ are larger than 0.15. The gain K_{p1} is selected so that the open-loop crossover frequency of the system, M_1/E_1, is equal to 2 rad/s. This is a representative value for a high-gain pilot control activity derived from flight test data [15]. When the gains for the first pair of loops have been determined, the same procedure is applied to the next 2nd-pair outer loop but with its open-loop crossover frequency reduced by a factor of 3 (0.667 rad/s for the 2nd-pair loop). This frequency separation is adopted to ensure that the outer loop exhibits a desirable integral-like behaviour around the outer-loop crossover frequency [1]. The same procedure is repeated until all of the necessary pilot gains are found.

If a multi-axis control situation is being considered, the gains of all of the rate-control loops in Figure 2 are reduced by a factor, *f*, modelling the task interference. The value *f* is given as follows [16;17],

$$f = 1 + 10(\sigma_{vis} + \sigma_{task}) \quad (3)$$

in which $\sigma_{task} = 0.01n$ if the number of control channels (n) is larger than one, else it will be zero. In addition, the aggressiveness of the pilot control activity can be modelled by multiplying the gains of all position-control loops with an aggression degree factor k_{agress}. Finally, the

vestibular and proprioceptive cues in Figure 1 illustrates the information perceived by the pilot.

2.2 Modelling of Pilot's Hazard Perception and Reaction

Successfully modelling piloting activities associated with hazard perception and reaction relies in understanding the following: the information that a pilot perceives and the control strategy that s/he takes to react to the impending hazard. These two issues are addressed in this Section.

2.2.1. Pilot Modelling of Hazard Perception

Hazard perception and its management is one important research branch of the broader process of pilot decision-making [20;21]. A hazard is a broad concept that can be defined as almost anything of actual or potential danger that requires a pilot to modify the current flight state e.g. altitude, airspeed, heading, route of flight, or configuration [13;20;21]. Hazards can be caused by internal and external factors as well as their combinations, such as knowledge or skills constrained by a pilot, adverse weather condition, performance limitation etc.

This paper focuses on a group of hazards - operationally imposed boundaries. For example, a pilot may encounter a situation whereby s/he is simultaneously trying to avoid a ground impact whilst, at the same time, preventing a low-altitude departure from controlled flight at an angle-of-attack limit. In this example, striking the ground is the potential hazard that might prevent the pilot from accomplishing this task. The following figure generalises this kind of hazard scenario.

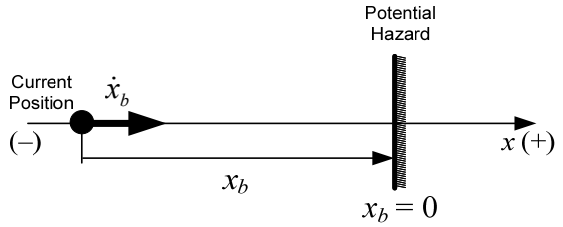

Figure 3 Illustration of imposed boundary hazards

Figure 3 shows that a vehicle is located at a distance (x_b) from a potential hazard whilst approaching it with an instantaneous velocity ($\dot{x}_b$).

Previous research has indicated that the tau (τ) information, based upon the perception of the instantaneous time-to-contact from the available optic flow when approaching an object or surface, provides a plausible means to model a human's perception and action for guiding movement [2;22-24]. This information also plays a vital role as a key parameter in the BAT model from the authors' previous work [25]. In this paper, optical τ is considered to be the primary information source used by a pilot to perceive and identify potential hazards.

The time-to-contact variable, τ, in the optical field [22], is defined as,

$$\tau_b = \frac{x_b}{\dot{x}_b} \tag{4}$$

which is based on the distance to boundary (x_b) at the current rate of approach ($\dot{x}_b$). This parameter models the pilot's perception of the time-to-contact the target (hereafter hazard), introduced by Lee [22] as a development of Gibson's optical flow theory of visual perception [26].

2.2.2. Pilot Modelling of Hazard Reaction

Describing pilot behaviour in the presence of a hazard is considered to be a complicated task [13]. There are three major theories to describe the potential reaction of a pilot in such circumstances: (1) Risk Homeostasis, proposed by Wilde [27], whereby people do not attempt to minimize risk; (2) Zero Risk theory proposed by Naatanen & Summala [28] whereby increasing experience will finally result in zero perceived risk. For example, a sufficiently experienced pilot will feel no real risk at all due to over confidence; (3) the threat avoidance model proposed by Fuller [29], whereby a trained pilot can learn to anticipate hazardous events and avoid adverse consequences. Since the research subjects in this paper are well-trained and skilled professional pilots, the threat avoidance model was adopted to investigate the possible actions of a pilot in response to the hazard of Figure 3. It is assumed that the pilot has correctly perceived the risk in this situation and will take appropriate HA actions in order to preserve the integrity of the flight task.

Two questions now arise as to when and how the pilot takes action to address the impending hazard(s). The current paper adopts the following pilot HA model proposed by Gray [25] to solve these two problems.

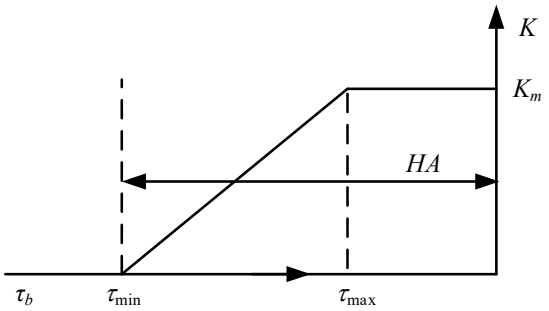

Figure 4 Pilot hazard-avoidance model with the time to boundary (τ_b)

The HA pilot model in Figure 4 is modelled as a function of control effort (K) to avoid the hazard, dependent on the variable τ_b (the instantaneous time to the hazards). τ_b is less (negatively) than the time (τ_{min}) at which a pilot first makes a control input in relation to the hazard. If the hazard continues to be approached, the control effort (K) increases linearly to its maximum, K_m. The control

effort is kept at this maximum level when the τ_b value is less than the time (τ_{max}) corresponding to the maximum control deflection. Therefore, the control effort increases linearly to its maximum, K_m, in the form

$$K = \frac{\tau_{min} - \tau_b}{\tau_{min} - \tau_{max}} K_m \quad (5)$$

This variable, τ_{min}, which is the time that the pilot starts to react to the hazard needs to be further elaborated upon. The determination of τ_{min} involves the pilot deciding whether or not to take an action when a hazard is perceived. This relates to the pilot's risk tolerance. This, in turn, is dependent upon the specifics of the situation and a large number of factors e.g. pilot experience and aircraft performance, but especially on the pilot's ability to perceive critical visual information [30]. For example, research into terrain following flight has shown that pilots rely on motion perception 6-8 seconds ahead [31], but only take action 2-3 seconds ahead. Moreover, a pilot with a high tolerance of risk will, in general, tend to be exposed to higher levels of risk [13]. This can result in a negative larger τ_{min}, indicating a late response to the perception of the hazard.

Using Eq. (5), it is hypothesized that the control effort increases linearly as the hazard is approached. However, Gray recognized that this process is likely to be non-linear in practice. It will be influenced by the complexity of the pilot's prospective control, the channels used to sense information, the flight control system and the aircraft dynamic characteristics. Moreover, the pilot may not always apply the maximum input available. When the pilot perceives that the hazard posed by the impending boundary is reducing, the control input is likely to be reduced to avoid other problems, such as reaching rate limits. Therefore, in reality, both $\tau_{\max}$ and K_m are likely to be 'adaptive' parameters depending on the situation.

The essence of HA pilot control effort variation is nonlinear due to the dependence on τ in Eq. (4) although it is modelled as a pure gain (K) in Eq. (5). This brings with it a difficulty in implementing Eq. (4) for analysing the stability of the closed-loop systems in Figure 1. It is proposed to address this nonlinearity issue by linearizing the information transfer characteristics of the HA attributes of the human controller. As illustrated in Figure 4, the pilot starts to take HA control effort when $\tau > \tau_{min}$. Therefore, Eq. (5) is linearized first using a Taylor series expansion at the initial state (x_{b0}, $\dot{x}_{b0}$) corresponding to the triggering moment ($\tau = \tau_{min}$) as shown in the following,

$$\tau(x_b, \dot{x}_b) \approx \tau(x_{b0}, \dot{x}_{b0}) + \dot{x}_{b0}^{-1}(x_b - x_{b0}) - x_{b0}\dot{x}_{b0}^{-2}(\dot{x}_b - \dot{x}_{b0}) \quad (6)$$

in which the higher-order terms are assumed to be noise in the perception process and therefore are ignored. The simplification of Eq. (6) yields the general solution,

$$\Delta\tau(x_b, \dot{x}_b) \approx \tau(x_b, \dot{x}_b) - \tau(x_{b0}, \dot{x}_{b0}) = \dot{x}_{b0}^{-1}\Delta x_b - x_{b0}\dot{x}_{b0}^{-2}\Delta\dot{x}_b \quad (7)$$

Finally, the Laplace transform of Eq. (7) can be described as follows,

$$\Gamma(s) = (\dot{x}_{b0}^{-1} - x_{b0}\dot{x}_{b0}^{-2}s)X(s) \quad (8)$$

in which $\Gamma(s)$ and $X(s)$ represent the Laplace transform of $\Delta\tau$ and Δx_b, respectively. Three points relating to the above procedure are worthy of note, as follows. Firstly, at the moment that the observer becomes aware of the existence of the hazard, the initial gap (x_{b0}) measuring the current distance to the hazard and the optical variable τ, by definition, is negative. However, the increments of both $\Delta\tau$ and Δx_b, as well as the hazard-approach speed ($\dot{x}_{b0}$), are positive. Secondly, the forms of solution given in Eqs. (7) and (8) that rely on $\Delta\tau$ are consistent with the finding of the recent study of information used in detecting upcoming collision (boundary) by Bootsma and Craig [32]. They found that the information carried in $\Delta\tau$ is the most effective predictor for collision avoidance. Finally, the perception of the optical tau information is modelled in Eq. (8) as introducing a lead equalization of the pilot. This lead term is entirely consistent with the prospective nature of the hypothesized τ-perception process in the optical field [22], i.e. a movement requires prospective control and the observer must have information about its future motion trajectory to be able to guide a movement successfully.

The above linearization at the moment of activation of the hazard feedback loop gives $\tau_{min} = \tau(x_{b0}, \dot{x}_{b0})$, as shown in Figure 1. After replacing τ in Gray's model in Eq. (5) with the linearized τ term, the following relationship can be determined,

$$K = (-\dot{x}_{b0}^{-1}\Delta x + x_{b0}\dot{x}_{b0}^{-2}\Delta\dot{x})\frac{K_m}{\tau_{min} - \tau_{max}} \quad (9)$$

in which the perception time delay τ_{dp} is temporarily ignored. The linear form of Eq. (9) can be transformed into the following and combined with τ_{dp}, in the Laplace plane thus.

$$K(s) = (T_{Lb}s + 1)K_b e^{-\tau_{db}s}X(s) \quad (10)$$

The final HA pilot model can be described in the form,

$$K(s) \approx \frac{T_{Lb}s + 1}{T_{lb}s + 1}K_b X(s) \quad (11)$$

in which $T_{Lb} = -x_{b0}\dot{x}_{b0}^{-1} = -\tau_{min}$, $K_b = \frac{-\dot{x}_{b0}^{-1}K_m}{\tau_{min} - \tau_{max}}$, and $\tau_{dp} = T_{lb}$. Moreover, it should be noted that $X(s)$ here is the distance to the hazard. Therefore, the HA feedback part of Gray's pilot model with the nonlinear τ variable can be approximately simplified into a lead-lag perception term. This brings with it the convenience of

the possibility of a closed-loop system stability analysis of Figure 1 in the presence of the hazard.

3. Experiment Setup

This Section describes the experimental setup designed to achieve the objectives stated in the Introduction Section.

3.1. Description of aircraft model and pilot-model development

The three degree-of-freedom (3DOF) longitudinal model used in this paper is linearized from the non-linear Bo105 model [33] at 80 kts and described as follows.

$$\dot{\boldsymbol{x}}(t) = \mathbf{A}\boldsymbol{x}(t) + \mathbf{B}\delta_{lon} \tag{12}$$

in which $\boldsymbol{x} = \begin{bmatrix} u & w & q & \theta \end{bmatrix}$. The variable u is the x-body axis velocity, w is the z-body axis velocity, q is the pitch rate, and θ is the pitch attitude. The matrices A and B have the following values:

$$\mathbf{A} = \begin{bmatrix} -0.0397 & -0.0012 & 5.9132 & -28.9264 \\ -0.0149 & -0.8543 & 140.9837 & 10.7268 \\ 0.0082 & 0.0318 & -5.5064 & -4.0324 \\ 0 & 0 & 0.9997 & 0 \end{bmatrix} \tag{13}$$

$$\mathbf{B} = \begin{bmatrix} -1.0278 \\ -3.2261 \\ 1.2680 \\ 0 \end{bmatrix} \tag{14}$$

Moreover, the neuromuscular damping ratio (ζ_{nm}) and natural frequency (ω_{nm}) in Figure 1 are selected as typical values of 0.707 and 10 rad/s, respectively [15;16]. The actuator for the longitudinal control input is selected as

$$G_{nm} = \frac{20^2}{(s+20)^2} \tag{15}$$

The simulation structure used for the investigation in this Section is shown in Figure 5.

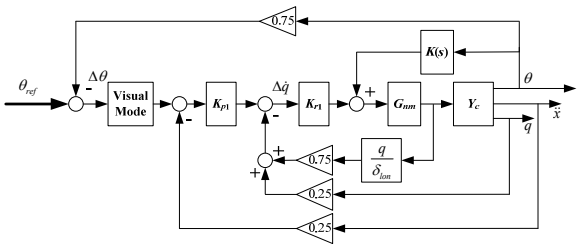

Figure 5 Pilot model for 3DOF pitch tracking task

The model of Figure 5 represents a motion-on flight simulation situation where the human pilot is now able to sense the vestibular and proprioceptive cues, such as the pitch rate and forward acceleration information. The transfer function in the proprioceptive feedback loop is as suggested in Ref. [17]. There, it recommends that the lowest-order model that matches the pitch-rate response with the longitudinal input be used. Moreover, the gain factors, with 0.75/0.25 split, asserted in Ref. [17;19] is used to weight the degree of the importance of each information channel in Figure 5.

The gains K_{p1} and K_{r1} are chosen to be 2.6 and 12.6, following the design guideline provided in Ref. [17]. The values for the parameters of the visual model and those that describe the aggressiveness of the pilot control behaviour are first selected to be: σ_{vis} = 0.02 (good visual simulation environment), f = 1.2 (no inter-axis coupling), and k_{agress} =1 (normal level of aggression).

3.2. Description of the Pitch Tracking Task

The experiment used for this work is illustrated in Figure 6.

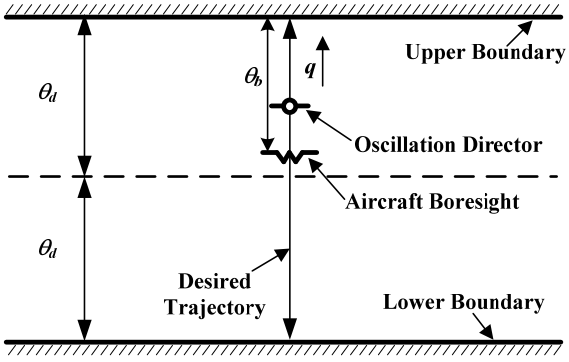

Figure 6 Illustration of a pitch tracking case with the boundary limits

The pitch tracking task of Figure 6 shows that the pilot (model) has to command the notional aircraft boresight symbol through the vehicle dynamics to capture a moving target (oscillation director). The impending hazard is modelled as the two boundaries shown [34]. The trajectory of the director is composed of four sinusoids as described in Eq. (16).

$$\sin(0.1\pi t) + 3\sin(0.05\pi t) + 2\sin(0.15\pi t) + 3\sin(0.3\pi t) \tag{16}$$

The experiment was also used for pilot-in-the-loop flight and this trajectory was used in order to try to reduce the predictability of the motion of the symbol. Moreover, the experiment designed in this section involves two considerations. The first relates to the failure of the tracking task. The case of hazard exceedance is considered as a fatal error [25]. Secondly, the PT pilot model will keep the same gain values (K_{r1} and K_{p1}) for the simulations with the parameters to be varied being τ_{min}, K_b, and θ_d. It is acknowledged that a pilot will adapt his dynamic behaviour, e.g. open-loop gain, effective time delay, and input remnant, as the demands of the task, environmental, and operator-centred variables change [10]. However, this does not violate the

methodology outlined above. The approach proposed here essentially focuses on what changes in both the pilot control behaviour and the tracking performance due to the HA process having been triggered. With the assumed constant PT pilot efforts, these possible changes will be exclusively associated with the variations of the HA parameters.

A series of boundary sizes with an optical viewing angle ranging between 6 and 15 degrees with an increment of one degree were selected to model the various levels of the difficulty of hazard avoidance, assuming that the smaller the boundary size, the greater the hazard level. The selection of these boundary sizes takes the minimum amplitude (about 6 degrees) of the desired designed signal into consideration.

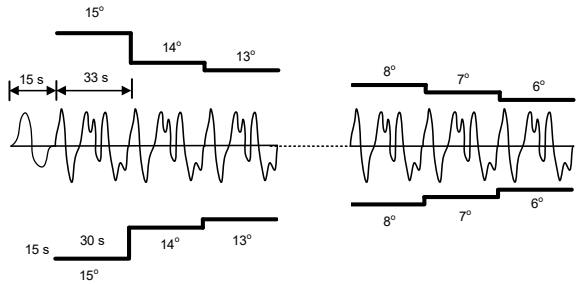

Figure 7 Illustration of hazards modelled as decreasing boundary size

The first 15 seconds of the experiment, shown in Figure 7, was used for pilot familiarization with the task. After this, the pitch-tracking task trajectory was repeated every 33s for each boundary. During each simulation run, only the longitudinal control channel was available to the pilot, the other three (lateral, collective, yaw pedals) had no influence on the model response.

The experimental study was conducted using the HELIFLIGHT-R simulator at The University of Liverpool [35]. The external and interior views of the simulator are shown in Figure 8.

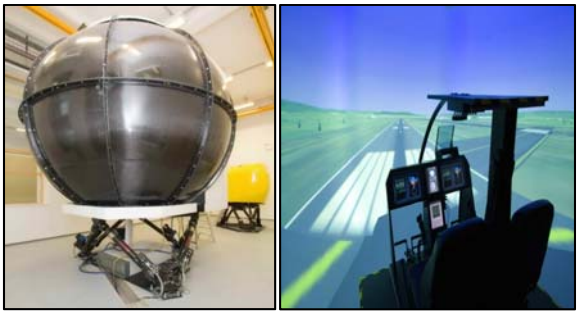

Figure 8 The external and interior views of HELIFLIGHT-R simulator [35]

The proposed closed-loop pilot model of Figure 5 was configured to represent the task conducted in the HELIFLIGHT-R simulator as shown in Figure 9.

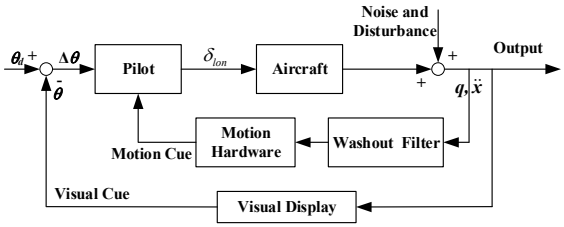

Figure 9 Illustration of the pilot-in-the-loop simulation in the HELIFLIGHT-R simulator

The following factors have been taken into account in implementing Figure 9 in the HELIFLIGHT-R simulator. Firstly, the same aircraft model and pitch tracking task will be used for theoretical analysis and piloted simulation. Moreover, because of the limited vertical Field of View within the HELIFLIGHT-R simulator, the range of the boundary size starting from 12 deg will be used for the piloted simulation, instead of 15 deg as used for the theoretical investigations. Secondly, for the 'motion-on' configuration, consisting of motion hardware and washout filters in Figure 9, only the surge acceleration ($\ddot{x}$) and the pitch rate (q) are fed to drive the motion base, which is consistent with Figure 5. For this task in-flight, it would be expected that there would also be non-trivial heave motion cues. These have not been included here because heave accelerations exist only in the collective loop of Hess' pursuit multi-loop model. However, for the purposes of this study, the omission of these cues did not matter per se, as they were neither included in the simulated flight test nor the model used to predict the results. Finally, the pilots were instructed to focus on the head-up display and ignore the display panel during the task. Meanwhile, the visual environment was covered by simulated thick fog in order to reduce the possibility of being disturbed by other visual stimuli. All of these measures were used to emphasize that the only visual cue perceived by the pilot will be the pitch attitude difference ($\Delta\theta$). Moreover, the pilots were instructed to use maximum effort to avoid an exceedance of the hazard limits. In the case that an exceedance occurred, the pilots were instructed to recover the situation promptly but to continue with the remainder of the task. Each pilot was required to repeat the task twice. The first run was used to familiarize the pilot with the task and the second was used for the reported analysis.

Three experienced pilots: A, B, and C, participated in the experiment. Pilot A is a commercial airline pilot and is an experienced test pilot. Pilot B is a retired Commercial Airline/British Royal Navy pilot. Pilot C is a current Apache pilot from a NATO Air Force. All pilots have undertaken extensive testing in rotary wing flight in both real flight tests and in simulation.

4. Results Analysis

4.1. Investigation of Pilot Reaction to a Hazard

Previous research has found that the gain and lead effort are the most important factors in the pilot dynamics that correlate with aircraft handling-quality evaluations [1]. For the pilot model shown in Eq. (11), the pilot gain and pilot lead are associated with K_b and $T_{Lb}(\tau_{min})$, respectively. Moreover, the main effect of the impending hazard (assuming the pilot needs to be aware of the hazard as assumed above) is that the pilot needs to immediately adopt a lead compensation control strategy to overcome it with an appropriate control gain. This effect is investigated first by searching the smallest critical K_b values (K_{bc}) that bring the closed-loop system (θ_{ref}/θ) to the neutral stability condition, with regard to various τ_{min} values (up to -10s). This is shown in Figure 10.

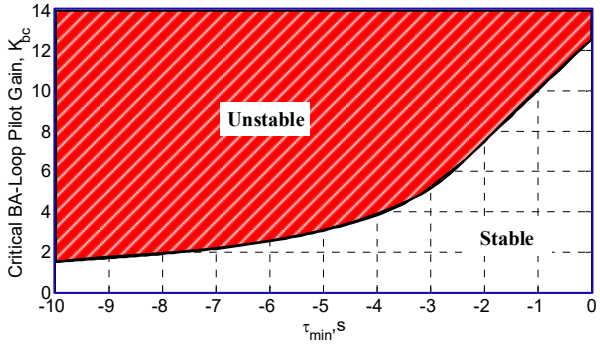

Figure 10 Variation of critical HA pilot gain with the HA initiation timing τ_{min}

Figure 10 is obtained with the τ_{min} range (-10, -0.2 s). The selection of this τ_{min} region is based upon the findings of previous research [25;36-39]. For example, research into terrain following flight has shown that the pilots rely on motion perception 6 - 8 seconds ahead but only take action 2 - 3 seconds ahead [31]. The BAT flight-based trials at the USAF TPS showed a typical τ_{min} range (-4, -1.0 s). Therefore, the expanded range (-10.0, 0.0 s) is selected for investigation here to give adequate coverage of all of the likely expected values. The perception time delay τ_{dp} value was selected to be 0.1 s [1;10]. As shown by Figure 10, the K_{bc} curve sharply increases as τ_{min} increases. This indicates that, the earlier the pilot initiates the HA process, the lower is the level of control margin (the stable range of the gain K_b) that will be available. This provides the pilot with less possibility of recovering from the influence of the approaching boundary. The primary reason for K_{bc} reducing as τ_{min} (negatively) increases is due to the fact that this situation requires more pilot control effort to generate a lead equalized visual cue, leaving less control margin available for other tasks. The increased amount of lead requirement actually increases the effective time delay of the pilot-vehicle system [1;10;40]. Under these situations, the pilot performance can be significantly affected.

The crossover frequency (ω_c) and the open-loop neutral stability frequency (ω_u, where the phase angle is –180° for the system in Figure 5) are plotted in Figure 11 with regard to the HA effort (K_b) and the timing of hazard recognition τ_{min}.

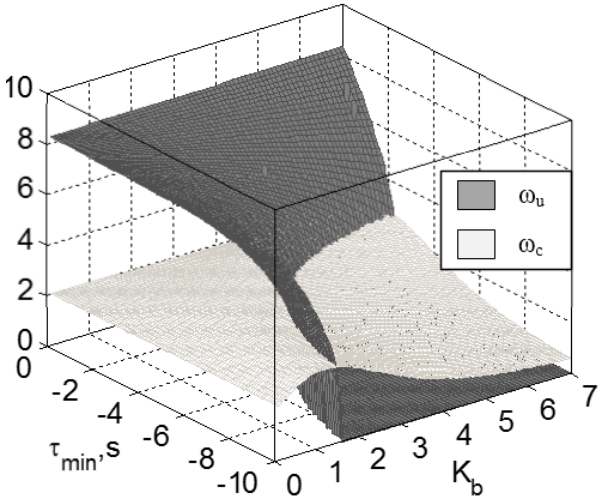

Figure 11 Closed-loop bandwidth against timing of hazard recognition and hazard avoidance effort

Figure 11 shows that the two bandwidth characteristic parameters decrease as K_b or τ_{min} (negatively) increases. This indicates reduced system stability. The cliff-like edge of the neutral stability bandwidth indicates the critical stability boundary of the open-loop system. Figure 11 shows that, with the additional HA feedback loop in Figure 5, the ω_c curve surface initiates from 2 rad/s, still complying with the design objective, and then stays at this value over a large region until crossing the ω_u surface as K_b and τ_{min} vary. This indicates that the HA loop has no significant influence on the pilot control activity (reflected by ω_c) and the consequent closed-loop tracking performance within this region. As K_b and τ_{min} increase, the ω_c surface slowly decreases but ω_u rapidly drops to zero. The good stability performance and wider bandwidth to some extents result from the increased number of cues being available in the latter case (in Figure 5) i.e. the inclusion of the vestibular and proprioceptive feedback loops. Refs. [1;10;41] have found that the availability of these cues can be attributed to a reduction in the effective time delay in the pilot perception channel and thus improves closed-loop stability performance because there is no need to generate angular rate or acceleration information by means of a lead equalized visual cue. These feedback loops can also be thought of as an inner loop which tends to reduce the effective operator time delay. Moreover, the authors in Ref. [42] have successfully modeled these cues as a negative pitch attitude feedback parallel to the main visual perception channel in their proposed pilot model.

The theoretical fatal and safe regions for each hazard size (6 – 15 deg) are illustrated in Figure 12.

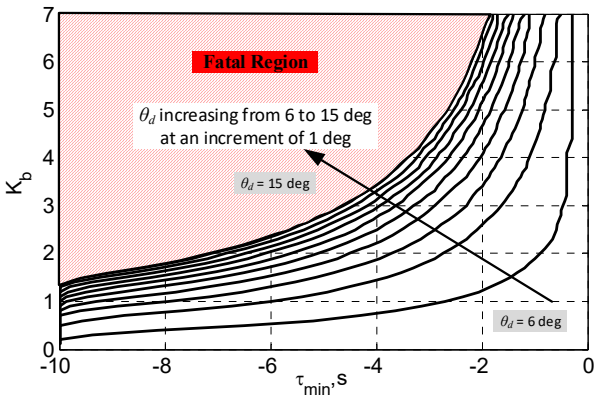

Figure 12 Fatal and safe region variation with hazard size

Figure 12 shows the profound influence of K_b and τ_{min} values on the safe flight region (entering into either system instability or violation of the boundary limit), subject to the various hazard levels. These figures show that the safe K_b - τ_{min} regions within the designated boundary size become larger as the boundary size increases. This indicates the fading influence of the increased boundary size on pilot control activity. Three interesting features are noted from Figure 12. Firstly, for the same τ_{min} value, the larger boundary size allows larger attainable pilot effort (K_b) and gives the pilot more control margin to avoid the impending boundary. This is especially reflected by the smaller τ_{min} values where there is no limitation on the K_b value that can be applied. This is actually a consequence of the HA process not being activated. The designed PT pilot model can ignore the boundary for a given boundary size where the τ_{min} values is relatively small (below a certain threshold). For example, for the designed experimental configuration, the boundary has no influence on the closed-loop tracking task when $\tau_{min} > -1.0$ s in the case of $\theta_d = 8$ deg, as shown in Figure 12. Moreover, the larger boundary size will result in a larger negative τ_{min} threshold. Secondly, compared with those in Figure 12, the proposed stability curve in Figure 10 follows a similar shape, but appears to be too conservative as expected, especially within the small τ_{min} range. The main reasons have been given above. However, the curve in Figure 10 is still useful because it illustrates the gross degree of the closed-loop system stability associated with the HA process, without requiring the prior knowledge of the desired tracking signal and the boundary size or other mission-specific details. Finally, for the same K_b value, the range that the modeled pilot maintains safety will decrease as τ_{min} becomes negatively larger. This is reasonable in that for the same boundary size, the negatively larger τ_{min} means more lead-equalization effort is required. This will increase the effective time delay, as discussed above.

With the derived safe region of Figure 10, the tracking performance for these boundary sizes is illustrated in Figure 13. The tracking performance is defined as the root-mean-squared (RMS) difference between the desired (Ref) and simulated (Sim) pitch attitude responses. The influence of the hazard on the pitch tracking performance are shown in Figure 13..

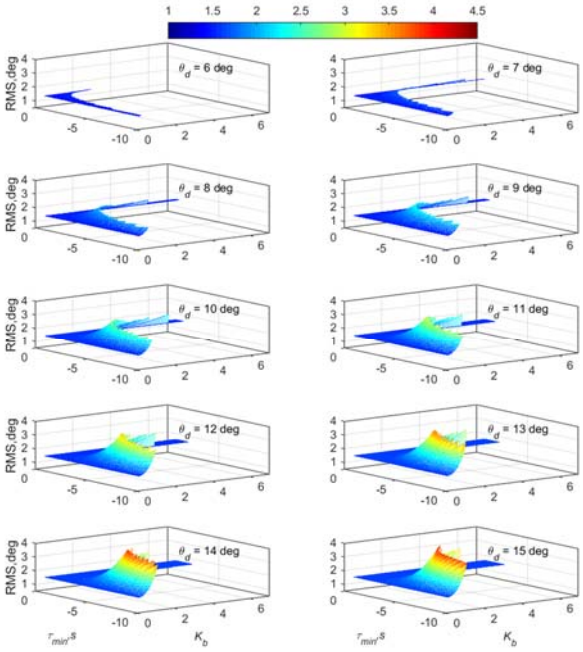

Figure 13 Tracking RMS variation with different K_b and τ_{min} values based on different hazard levels

The effects of the different hazard levels on the achieved tracking performance can be summarized from Figure 13 as follows. Firstly, because the positive feedback property of the HA loop has a significant influence on the closed-loop stability (Figure 10 to Figure 12), it is expected that the larger positive feedback effort of the inner loop will result in a larger tracking error, resulting from the reduced open-loop and closed-loop bandwidths. The distribution of the tracking RMS performance in Figure 13 (referring to non-blue zones) confirms this expectation as K_b increases. This finding can be used to explain the phenomenon found in Refs. [36-38] for fixed-wing aircraft, whereby the tracking performance slightly improves as the hazard level decreases.

An apparent phenomenon when the pilot operates in the blue region of Figure 13 associated the smaller negative τ_{min} is that a smaller boundary size can increase the tracking performance. This is worthy of discussion. The previous study has assumed that, for the same task under the same flight condition, a pilot adopts the same τ_{min} value. As shown in Figure 10, the decreasing boundary size will compel the pilot to adopt a smaller K_b value to maintain safe flight. In turn, this will have a lesser effect on the outer closed-loop tracking performance. This phenomenon is also reflected by the points within the region denoted by the blue color in Figure 13 (those τ_{min} - K_b pairs in the common safe region in Figure 10). These points show that tracking performance slightly

improves by approximately 6%, as the boundary size decreases. For example, the RMS value is around 1.58 deg at θ_d = 6 deg but 1.7 deg at θ_d = 15 deg. However, the benefits from the boundary-size reduction will not always necessarily be evident. Not only can the smaller boundary size result in a narrower safe region in Figure 10, but the tracking performance will be worse, shown by the narrowed-blue region in Figure 13. Therefore, the tracking RMS values with smaller boundary sizes will be larger than those still not affected. Furthermore, previous studies [36-38] also found that the tracking performance will degrade when a certain 'critical' boundary size is reached and this can even lead to BAT-PIO situations as reported in Ref. [9]. This primarily results from the reduced control margin for the smaller boundary size that makes the pilot more susceptible to system safety maintainability problem (smaller safer region) as illustrated in Figure 10. If the boundary size is too narrow, for the same τ_{min} value, a small increase in K_b as the boundary approaches will cause a violation of the safe region.

Finally, the studies in this Section have modeled the HA feedback as positive resulting from the increased lead-equalization control effort used by the human operator due to the impending boundary, through Eq. (11). Moreover, the results above have demonstrated that the extra HA efforts correlate with a reduction in the open-loop frequency bandwidths (in Figure 11) and the influence of the HA loop on the closed-loop stability and tracking performance equally increases the effective time delay.

4.2. Validation of PT Pilot Model

Two metrics - the cutoff frequency values (ω_{cut}) and the amplitude of the tracking-error RMS are used to validate the multi-loop PT pilot model, based on the piloted-simulation results in Figure 14. In these figures, the cutoff frequency (ω_{cut}) is adopted to measure the frequency of pilot control activity applied in this Section [43]. The method used to calculate its value is shown in Appendix A.

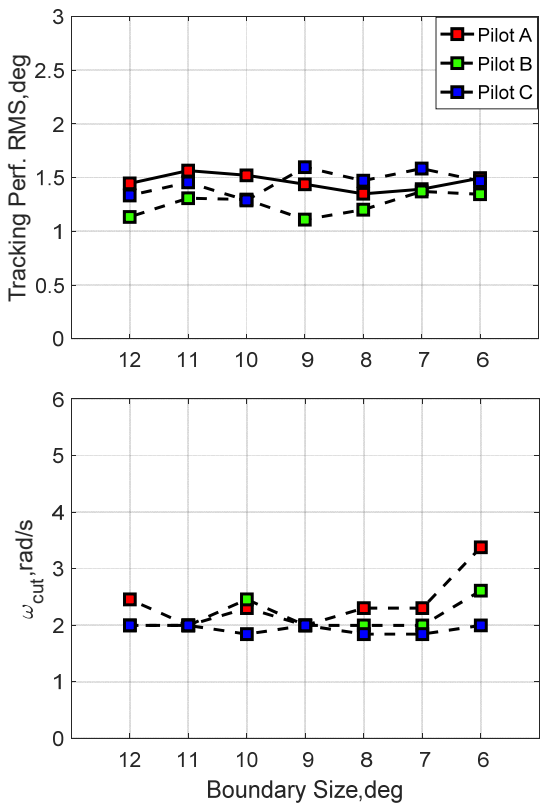

Figure 14 Illustration of tracking performance and pilot control characteristics

The cutoff-frequency values (ω_{cut}) of all pilots obtained from experiments generally approach the desired baseline value 2 rad/s used to build the PT pilot model. This indicates all three pilots tended to adopt similar control bandwidth, in spite of the different imposed boundaries. This shows that the baseline value used in Figure 5 is a representative number that reflects real pilot's control activity. Moreover, all three pilots appear to apply more control at the smallest boundary size (6 deg). The cutoff frequency value of Pilot A even increases to 3.3 rad/s. This indicates that the impeding hazard at this level has a significant influence on this pilot's control activities, as it does for Pilot B.

The second metric is based on the tracking RMS values in Figure 13 and Figure 14. The tracking performance in Figure 14 varies by approximately 10% of their individual mean values for all pilots. The smaller motion-on tracking-performance variation, with all around the similar mean value (1.6 deg) for all three pilots, as the boundary size varies is in line with the prediction of Figure 13. This is likely due to the pilots choosing τ_{min} and K_b values in the blue region of Figure 13 in which the tracking performance is not particularly susceptible to the adaption of the control input (K_b). Moreover, it is worth pointing out that the predicted tracking RMS values (1.58 – 1.7 deg mentioned above) in the blue region of Figure 13 across the different boundary sizes from the pilot model in Figure 5 are very

close to the experimental values of pilot simulation (1.3 – 1.7 deg) in Figure 14. This is regardless of the fact that only generic, representative values were used to configure the pilot model, e.g., the neuromuscular model in Eq. (1). Therefore, it is reasonable to draw the conclusion that the pilot model structure that consists of the PT and HA parts proposed in this paper to some extent represent the actions of a real professional pilot. The minor differences between the piloted-simulation results and the theoretically predicted values can mainly be ascribed to the following two reasons. First, as mentioned earlier, the neuromuscular model used in Figure 5, presents a generalized, idealized and appropriate human property, but not necessarily one that is fully representative of the specific pilots involved in the experiments. The other values used in Figure 5 also are not specified for a particular pilot. Second, there are still a number of other factors that can degrade the performance of the human pilots, such as fatigue, which are not modelled in the PT pilot model. Moreover, the motion cues sensed by the real pilots are slightly different from those assumed for the pilot model in that they experience the full motion instead of the motion cues limited in the longitudinal channel implemented in this paper.

4.3. Investigations of Pilot Control Efforts

The control effort of the three pilots whilst performing the pitch tracking task are illustrated in Figure 15 in terms of amplitude RMS values.

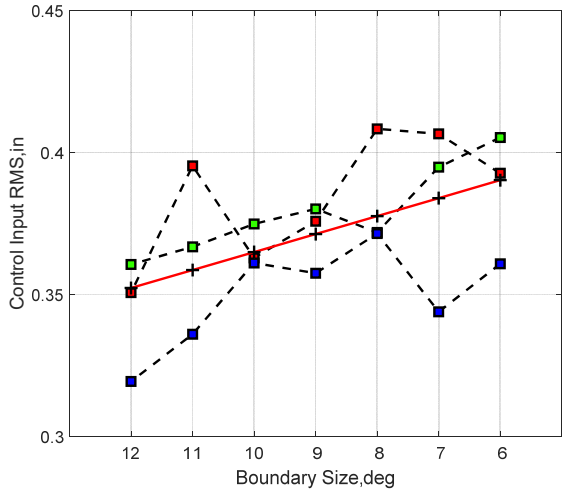

Figure 15 Illustration of pilot control effort against the varying boundary size

A similar explanation as given above for the tracking performance analysis can be applied to the smaller control input variation (<10%) with similar mean values (≈ 0.37 in) shown in Figure 15. As shown in Figure 11, the wide flat ω_c region in Figure 11 indicates the pilot input will be roughly constant under larger variation with K_b (HA control efforts) and τ_{min} (different pilots). Moreover, the effects imposed by the hazard can also be partially observed in Figure 15. Compared with the influence of the hazard on the performance, its effects on the pilot control inputs appear to be consistently and slightly increasing on average. All pilots tend to slightly increase their control effort to maintain a similar tracking performance as the hazard level increases. For example, Pilot A and Pilot B generally increase control effort as the boundary size reduces, and Pilot C increases first and then drops at 7 deg and increases again at 6 deg.

5. Conclusions

This paper has reported upon the creation and subsequent analysis of a pilot model that combined both a PT and HA elements. The following conclusions have been drawn from the work presented. Firstly, the PT pilot model developed in the previous research has been validated using real piloted-simulation data conducted by three professional pilots. The theoretical results have reached good agreement with the real simulation results in terms of the cut-off frequency and the tracking RMS value. Second, the research presented in this paper quantitatively reveals the essence of the pilot reaction mechanism to a hazard to be equivalent to the addition of a time delay and the adaption of the control gain. The severity of the HA situation is dependent upon the amount of visual lead equalization and associated control gain applied by the pilot. The effects of a HA task on the closed-loop system can be investigated by mathematically modelling it as a positive feedback lead-lag term. Third, the research shows that the pilots tend to increase their control effort to maintain the tracking performance when the hazards become more severe. Conversely, as the hazards become more benign, the pilot has more freedoms in term of choosing τ_{min} - K_b pairs to achieve the similar tracking performance.

Acknowledgements

The research leading to these results has received funding from the European Community's Seventh Framework Programme (FP7/2007-2013) under grant agreement N° 266073.

Reference

[1] McRuer, D. T., et al., *Aviation Safety and Pilot Control Understanding and Preventing Unfavourable Pilot-Vehicle Interactions*, National Academy Press, ASEB National Research Council, Washington D.C., 1997.

[2] Padfield, G. D., "Flying Qualities: forms of degradation", *Helicopter Flight Dynamics,* 2nd ed., Blackwell Science, Oxford, 2007, pp. 517-559. doi: 10.1002/9780470691847.ch8

[3] Hess, R.A., "Unified Theory for Aircraft Handling Qualities and Adverse Aircraft - Pilot Coupling," *Journal of Guidance, Control, and Dynamics*, published online Nov. 1997; Vol. 20, No. 6, pp. 1141-1148. doi: 10.2514/2.4169

[4] Pavel, M. et al., “Practices to Identify and Preclude Adverse Aircraft-and-Rotorcraft-Pilot Couplings – A Design Perspective,” *Progress in Aerospace Sciences*, July 2015, Vol. 76, pp 55–89. DOI: 10.1016/j.paerosci.2015.05.002

[5] S. Neumark, "Problems of Longitudinal Stability below Minimum Drag Speed, and Theory of Stability under Constraint," HMSO London, ARC/R&M-2983 ARC-16825 RAE/Aero-2504, 1953.

[6] Lu, L., Padfield, G. D., and Jump, M., “Investigation of Rotorcraft-Pilot Couplings under Flight-Path Constraint below the Minimum-Power Speed,” *Aeronautical J*, published online July.2010, Vol. 114, No. 1157, pp. 405-416.

[7] M. L. Mohammad and K. C. Alastair, "Review of Pilot Modelling Techniques," 48th AIAA Aerospace Sciences Meeting, AIAA 2010-297, 4-7 Jan.2010, Orlando, Florida, pp. 1-16.

[8] Gray III, W. R., "Boundary-Escape Tracking: A New Conception of Hazardous PIO," Technical paper, Air Force Flight Test Center, EDWARDS AFB CA, Sep 2004.

[9] Lu, L., and Jump, M. “Multiloop Pilot Model for Boundary-Triggered Pilot-Induced Oscillation Investigations,” *Journal of Guidance, Control, and Dynamics*, published online, 2014, Vol. 37, No. 6, pp. 1863-1879. doi:10.2514/1.G000079.

[10] McRuer, D. T., Clement, W. F., Thompson, and R. E. Magdaleno, "Minimum Flying Qualities Volume II: Pilot Modelling for Flying Qualities Application," Flight Dynamics Laboratory, Air Force Systems Command, Wright-Patterson Air force Base, OHIO, WRDC-TR-89-3100, Jan.1990.

[11] Allen, R. W., Clement, W. F., and Jex, H. R., “Research on Display Scanning, Sampling, and Reconstruction Using Separate Main and Secondary Tracking Tasks,” NASA Contractor Report CR-1569, NASA Contractor Report CR-1569, Jul. 1970.

[12] Anon., “Aeronautical Design Standard Performance Specification Handling Qualities Requirements for Military Rotorcraft”, ADS-33E-PRF, US Army Aviation and Missile Command, Aviation Engineering Directorate, Redstone Arsenal, Alabama, Mar. 2000.

[13] Hunter, D. R., "Risk Perception and Risk Tolerance in Aircraft Pilots," DOT/FAA/AM-02/17, FAA, Office of Aerospace Medicine, Washington, DC 20591, Sept.2002.

[14] Anon., "Annual Safety Review 2016," EASA, D-50668 Cologne, Germany, July2016.

[15] Hess, R.A., “Simplified Approach for Modelling Pilot Pursuit Control Behaviour in Multi-Loop Flight Control Tasks,” *Proceedings of the I MECH E Part G Journal of Aerospace Engineering*, published online 2006; Vol. 220, No. 2, pp. 85-102. doi: 10.1243/09544100JAERO33

[16] Hess, R.A., “Obtaining Multi-Loop Pursuit-Control Pilot Models from Computer Simulation,” *Proceedings of the I MECH E Part G Journal of Aerospace Engineering*, published online Feb. 2008; Vol. 222, No. 2, pp. 189-199. doi: 10.1243/09544100JAERO260

[17] Hess, R. A., and Marchesi, F., “Analytical Assessment of Flight Simulator Fidelity Using Pilot Models,” *Journal of Guidance, Control, and Dynamics*, published online May. 2009; Vol. 32, No. 3, pp. 760-770. doi: 10.2514/1.40645

[18] Hess, R.A., and Stout, P. W., “Assessing Aircraft Susceptibility to Nonlinear Aircraft-Pilot Coupling/Pilot-Induced Oscillations,” NASA/CR-97-207296, 1997.

[19] Hess, R.A., and Siwakosit, W., “Assessment of Flight Simulator Fidelity in Multiaxis Tasks Including Visual Cue Quality,” *Journal of Aircraft*, published online Jul. 2007; Vol. 38, No. 4, pp. 607-614. doi: 10.2514/2.2836

[20] Green, M. F., "Aviation System Safety and Pilot Risk Perception: Implications for Enhancing Decision-Making Skills," *Journal of Air Transportation World Wide*, 2001, Vol. 6, No. 1, pp. 98-111.

[21] Hunter, D. R., "Risk Perception and Risk Tolerance in Aircraft Pilots," *The International Journal of Aviation Psychology*, 2006, Vol. 16, No. 2, pp. 135-144.

[22] Lee, D. N., “Guiding Movement by Coupling Taus,” *Ecological Psychology*, published online 1998; Vol. 10, No. 3, pp. 221-250. doi:10.1207/s15326969eco103&4_4

[23] Keil, M. S, and López-Moliner, J., "Unifying Time to Contact Estimation and Collision Avoidance across Species," *PLoS Comput Biol*, Aug.2012, Vol. 8, No. 8, pp. 1-13.

[24] Padfield, G. D., “The Tau of Flight Control,” *Aeronautical Journal*, published online Sept. 2011; Vol. 115, No. 1171, pp. 521-555.

[25] Gray III, W. R., “Boundary-Avoidance Tracking: A New Pilot Tracking Model,” *AIAA Atmospheric Flight Mechanics Conference and Exhibit*, San Francisco, California, Aug., 2005, pp. 86-97.

[26] Gibson, J. J., “The Perception of the Visual World,” *American Journal of Psychology*, Vol. 64, 1951, pp. 622-625.

[27] R. M. Trimpop and G. J. S. Wilde, Challenges to Accident Prevention: The Issue of Risk Compensation Behaviour Groningen, The Netherlands: Styx Publications, 1994.

[28] Naatanen, R., and Summala, H. “A Model for the Role of Motivational Factors in Drivers' Decision-Making,” *Accident Analysis and Prevention*, 1974, pp. 243-261.

[29] Fuller, R., "A Conceptualization of Driving Behaviour as Threat Avoidance," *Ergonomics*, 1984, Vol. 27, No. 11, pp. 1139-1155.

[30] S. Oppe, "The Concept of Risk: A Decision Theoretic Approach," *Ergonomics*, 1988, Vol. 31, No. 4, pp. 435-440.

[31] Padfield, G. D., Lee, D. N., and Bradley, R., "How Do Helicopter Pilots Know When to Stop, Turn or Pull Up?," *Journal of the American Helicopter Society*, published online 2003; Vol. 48, No. 2, pp. 108-119. doi: 10.4050/JAHS.48.108

[32] Bootsma, R. J., and Craig, C. M., "Information Used in Detecting Upcoming Collision," Perception, published online 2003; Vol. 32, No. 5, pp. 525-544. doi: 10.1068/p3433

[33] Jones, M., Jump, M., Lu, L., Pavel, M., and Yilmaz, D., "The Use of the Phase-Aggression Criterion for Identification of Rotorcraft Pilot Coupling Events," *38th European Rotorcraft Forum*, Amsterdam, Netherlands, Sept. 4th-7th 2012.

[34] Pavel, M. D., and et al., "Adverse Rotorcraft-Pilot Couplings - Prediction and Suppression of Rigid Body RPC," *34th European Rotorcraft Forum*, Liverpool, England, Sept. 16th -18th 2008.

[35] M. D. White, P. Perfect, G. D. Padfield, A. W. Gubbels, and A. C. Berrayman, "Acceptance Testing of a Rotorcraft Flight Simulator for Research and Teaching: the Importance of Unified Metrics," in 35th European Rotorcraft Forum, Hamburg, Germany 2009.

[36] Blake, R.D. *Boundary Avoidance Tracking: Consequences (and Uses) of Imposed Boundaries on Pilot-Aircraft Performance*, MSc Thesis, Department of the Air Force, United States Air Force Institute of Technology, Wright-Patterson Air Force Base, Ohio, 2009.

[37] Dotter, J. D., "An Analysis of Aircraft Handling Quality Data Obtained from Boundary Avoidance Tracking Flight Test Techniques," Air Force Inst. of Tech., Wright-Patterson AFB, OH. Graduate School of Engineering and Management, Mar. 2007.

[38] Gray III, W. R., "Handling Qualities Evaluation at the USAF Test Pilot School," Proceedings of the AIAA Atmospheric Flight Mechanics Conference 10 - 13 August 2009, Chicago, Illinois.

[39] Warren, R. D., "An Investigation of the Effects of Boundary Avoidance on Pilot Tracking," Air Force Inst. of Tech., Wright-Patterson AFB, OH. Graduate School of Engineering and Management, Dec., 2006.

[40] McRuer, D. T., "Pilot-Induced Oscillations and Human Dynamic Behavior," NASA Contractor Report 4683, Jul.1995.

[41] McRuer, D. T., and Jex, H. R., "A Review of Quasi-Linear Pilot Models," *IEEE Transactions on Human Factors in Electronics*, published online Sept. 1967; Vol. 8, No. 3, pp. 231-249. doi: 10.1109/THFE.1967.234304

[42] Zaal, P. M. T., Pool, D. M., Van Paassen, M. M., and Mulder, M., "Comparing Multimodal Pilot Pitch Control Behavior Between Simulated and Real Flight," *Journal of Guidance, Control, and Dynamics*, published online Sept. 2012; Vol. 35, No. 5, pp. 1456-1471. doi: 10.2514/1.56268

[43] Klyde, D. H., Schulze, P. C., Thompson, P. M., and Liang, C. Y., "Use of Wavelet Scalograms to Characterize Rotorcraft Pilot-Vehicle System Interactions," *Proc. of 67th AHS*, Virginia Beach, VA, May 2011.

Appendix A

The classical pilot cutoff frequency (ω_{cut}) is defined as the frequency point at which the RMS value of the input signal (ψ_1) from the frequency range of $0 - \omega_1$, is equal to the half of the total RMS of this signal (ψ_{tot}), as follows,

$$\frac{\psi_{cut}^2}{\psi_{tot}^2} = 0.5 \tag{A1}$$

in which

$$\psi_{tot}^2 = \frac{1}{2\pi}\int_0^{\infty} G_{\delta\delta} d_{\omega} \text{ and } \psi_1^2 = \frac{1}{2\pi}\int_0^{\omega_1} G_{\delta\delta} d_{\omega} \tag{A2}$$

and $G_{\delta\delta}$ is the auto spectrum of the signal, which is normally obtained the standard Fourier transform.